Exciton Delocalization Drives Rapid Singlet Fission in Nanoparticles of Acene Derivatives

Ryan D. Pensack,[†,∥] Andrew J. Tilley,[†,∥] Sean R. Parkin,[‡] Tia S. Lee,[†] Marcia M. Payne,[‡] Dong Gao,[†] Ashlee A. Jahnke,[†,#] Daniel G. Oblinsky,[§] Peng-Fei Li,[†] John E. Anthony,*[‡] Dwight S. Seferos,*[†] and Gregory D. Scholes*[†,§]

[†]Department of Chemistry, University of Toronto, Toronto, Ontario M5S 3H6, Canada
[‡]Department of Chemistry, University of Kentucky, Lexington, Kentucky 40506, United States
[§]Department of Chemistry, Princeton University, Princeton, New Jersey 08544, United States

Ⓢ *Supporting Information*

ABSTRACT: We compare the singlet fission dynamics of five pentacene derivatives precipitated to form nanoparticles. Two nanoparticle types were distinguished by differences in their solid-state order and kinetics of triplet formation. Nanoparticles that comprise primarily weakly coupled chromophores lack the bulk structural order of the single crystal and exhibit nonexponential triplet formation kinetics (Type I), while nanoparticles that comprise primarily more strongly coupled chromophores exhibit order resembling that of the bulk crystal and triplet formation kinetics associated with the intrinsic singlet fission rates (Type II). In the highly ordered nanoparticles, singlet fission occurs most rapidly. We relate the molecular packing arrangement derived from the crystal structure of the pentacene derivatives to their singlet fission dynamics and find that slip stacking leads to rapid, subpicosecond singlet fission. We present evidence that exciton delocalization, coincident with an increased relative admixture of charge-transfer configurations in the description of the exciton wave function, facilitates rapid triplet pair formation in the case of single-step singlet fission. We extend the study to include two hexacene derivatives and find that these conclusions are generally applicable. This work highlights acene derivatives as versatile singlet fission chromophores and shows how chemical functionalization affects both solid-state order and exciton interactions and how these attributes in turn affect the rate of singlet fission.
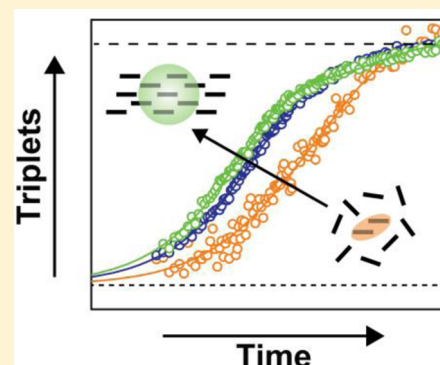
INTRODUCTION

Singlet exciton fission is a spin-allowed energy conversion process whereby a singlet excited chromophore (S_1) couples to an adjacent ground state chromophore (S_0) to yield two triplet excitons ($T_1 + T_1$).[1−3] The phenomenon was originally observed in the 1960s in crystals of anthracene and tetracene.[1,2] Following many years of near dormancy in terms of research activity (see ref 2 and refs therein), interest has recently surged due to the recognition that this process represents a potential means to circumvent the thermodynamic limitations of single-junction photovoltaic cells.[4−7] Specifically, the energy of a singlet exciton in excess of the optical gap that would otherwise be thermalized prior to charge separation is retained by splitting the photogenerated singlet exciton into a pair of triplet excitons. The resultant pair of triplet excitons can subsequently undergo charge separation at an interface with a suitable organic or inorganic electron acceptor,[8−13] potentially leading to external quantum efficiencies exceeding 100%.[10,11,14,15] In order to achieve high photovoltaic conversion efficiencies, this approach requires the electron acceptor also absorb low energy photons and that these photogenerated excitons undergo charge separation such that the overall spectral response is enhanced.[6,7] In this way, a device incorporating a singlet fission sensitizer can be considered a tandem device in a single junction.[2]

A critical intermediate in the singlet fission mechanism is the correlated triplet pair, denoted $^1(TT)$, which can be described by a superposition of triplet pair states that exhibits overall singlet character.[1−3] Thus, the interconversion of the singlet exciton, $|S_1\rangle|S_0\rangle$, and correlated triplet pair is a spin-allowed process. The pairwise rate of forming the correlated triplet pair depends on the strength of the coupling matrix element between the singlet exciton and the correlated triplet pair.[2,16] Under conditions favorable for separation, the correlated triplet pair converts into localized, isolated triplets.

Only certain organic materials undergo singlet fission.[2,16,17] The most general requirement of a singlet fission chromophore is energy conservation, i.e., the first-excited singlet state must be greater than or equal to twice the energy of the lowest triplet state (i.e., $E(S_1) \geq 2 \times E(T_1)$). Singlet fission chromophores that are the most intensively investigated include the

polyacenes, perylenes, carotenoids, and conjugated polymers (see refs 2 and 16 and refs therein). Tetracene, pentacene, and hexacene are particularly favorable as singlet fission in crystals and thin films of these compounds exhibit triplet yields approaching 200%.[18−24] Notably, a triplet yield in excess of 100% has been reported in largely amorphous films of a tetracene derivative that exhibits singlet fission.[25] Triplet yields approaching 200% are not exclusive to the polyacenes, however, as yields of this order have been reported in zeaxanthin aggregates[26] as well as in thin films of 1,3-diphenylisobenzofuran[27,28] and a perylenediimide derivative.[29] Of the polyacenes, each has certain advantages and disadvantages associated with considerable variation in their respective triplet energies and singlet fission rates.[2,24,30] Pentacene and its derivatives, for example, exhibit notably rapid singlet fission as a result of optimal exoergic conditions.[24,30] In the simplest picture, the relative rates of various dynamical processes govern the overall efficiency,[31] and therefore one can infer the overall efficiency of a particular process from the relative rates.[18,22,24,31] Rapid singlet fission is particularly advantageous because singlet fission must kinetically outcompete alternate excited-state decay pathways and energy conversion processes such as excimer formation and charge separation.[2,16]

The physical arrangement of a pair of molecules, i.e., their relative orientation and displacement, is expected to significantly influence singlet fission dynamics.[2,16] Recent theoretical work on perylenediimide[32] and pentacene derivatives[33] has indicated that singlet fission dynamics depend sensitively on the arrangement between pairs of molecules. As such, it would be advantageous to be able to reliably control molecular arrangement in order to develop structure−function relationships relevant to singlet fission. Efforts to systematically control molecular arrangement originally targeted covalently tethered molecular pairs; however, triplet yields much lower than solid films of the parent compounds were observed.[18,19,27,28,34−38] The origin of the low triplet yield was ultimately attributed to geometric factors nonoptimal for singlet fission in covalently tethered molecules,[36,37] and the effect of molecular arrangement on singlet fission dynamics remained unclear. Two studies on covalently tethered cofacial and slip-stacked perylenediimide derivatives excluded singlet fission as a probable excited-state decay pathway,[39,40] even when varying the displacement of the covalently tethered perylenediimides.[39] Most recently, work on covalently tethered pentacene pairs has been reported that highlights the sensitivity of singlet fission dynamics on electronic coupling.[41] Extending these pioneering works to studies in the solid state is critical to gaining insight into fundamental aspects of the singlet fission mechanism.

Solid-state order imparts considerable influence on singlet fission dynamics. The physical arrangement of molecules in a solid determines the properties of excitons,[42] including the extent of delocalization and associated relative admixture of charge-transfer (or ionic) configurations in the description of the exciton wave function.[43,44] These attributes, in turn, are reflected in the exciton energy as well as the extent of electronic coupling between chromophores—both key parameters that govern singlet fission rates and efficiencies.[2,16,24,30,45] The most recent experimental work investigating the influence of solid-state order on singlet fission dynamics include a study on a thin film of a slip-stacked perylenediimide derivative,[29] a study on two crystal polymorphs of 1,6-diphenyl-1,3,5-hexatriene,[45] work on two crystal polymorphs of 1,3-diphenylisobenzofuran,[28,36,46]

and a joint theoretical and experimental study on dimers and films of a series of acenes and acene derivatives.[30] It has recently been suggested that collective effects owing to exciton delocalization play a role in singlet fission dynamics.[47] Such effects are difficult to calculate, so experimental input is needed.

Since the original work of Kasai et al.,[48] a number of research efforts have been directed at utilizing aggregate solutions as an alternative medium in which to investigate photochemistry[49−58] and photophysics[26,59−65] in molecular solids. Previous studies on aggregates of singlet fission chromophores have highlighted the ability to gain insight into exciton properties and singlet fission dynamics.[26,49,59,63−65] Herein, we investigate aqueous colloidal nanoparticle suspensions[64] of a class of materials designed for molecular crystal engineering.[66−68] The compounds are 6,13-bis(tri*iso*propylsilylethynyl)pentacene (TIPS-Pn), 6,13-bis(tri*sec*butylsilylethynyl)pentacene (TSBS-Pn), 6,13-bis(tri*iso*butylsilylethynyl)pentacene (TIBS-Pn), 1,2,3,4,8,9,10,11-octafluoro-6,13-bis(*n*-octyldi*iso*propyl-silylethynyl)pentacene (F8-NODIPS-Pn), and a statistical mixture of 2,9- and 2,10-dibromo-6,13-bis-(tri*iso*propylsilylethynyl)pentacene (Br2-TIPS-Pn). Three of the derivatives, TIPS-, TSBS-, and TIBS-Pn, differ by at most one methylene group in their side chains, while F8-NODIPS-Pn and Br2-TIPS-Pn enable us to investigate the effect of core halogenation on singlet fission dynamics. We extend the study to two similarly functionalized halogenated hexacene (Hn) derivatives. We find that acene derivatives are versatile singlet fission chromophores and that solid-state order and exciton delocalization promote rapid singlet fission.

■ EXPERIMENTAL METHODS

Pentacene Derivatives. HPLC-grade (≥99%) TIPS-Pn was purchased from Sigma-Aldrich and used as received. The other Pn derivatives were synthesized as reported in the literature.[69,70]

Nanoparticle Preparation. 200 μL of an 800 μM solution of the acene derivative in reagent-grade tetrahydrofuran (THF; Sigma-Aldrich, St. Louis, Missouri) was rapidly injected into a 20 mL glass scintillation vial (Kimble Chase, Vineland, New Jersey) containing 10 mL of vigorously stirring distilled water. A 21 gauge disposable needle (BD, Franklin Lakes, New Jersey) and 1 mL disposable syringe (Henke-Sass Wolf, Tuttlingen, Germany) were used to inject the acene derivative/THF solution. To facilitate the evaporation of residual THF following injection, the resultant aqueous colloidal acene derivative nanoparticle suspension was (i) kept stirring at room temperature while exposed to the atmosphere for a period of several hours, (ii) kept stirring at room temperature while exposed to the atmosphere and bubbling nitrogen gas through the solution for 30−60 min, or (iii) subjected to rotary evaporation at 75 mbar and 40 °C for 30 min. A Hei-VAP Precision rotary evaporator (Heidolph North America, Elk Grove Village, Illinois) was used for the rotary evaporation. For the pump−probe measurements, concentrated aqueous colloidal nanoparticle suspensions were prepared by combining three 10 mL batches together and subjecting the total solution to rotary evaporation at 50 mbar and 40 °C for a period of ~1 h. Concentrated aqueous nanoparticle suspensions were passed through a 0.2 μm pore size syringe filter (Sarstedt, Nümbrecht, Germany) before measurements.

Steady-State Absorption Spectroscopy. Absorption spectra were measured with either a Varian Cary 100 Bio spectrophotometer (Varian Medical Systems, Inc., Palo Alto, CA) or an Agilent Cary 6000i UV−vis-NIR spectrophotometer (Agilent Technologies, Santa Clara, CA) equipped with an integrating sphere detector (in the case of aqueous colloidal Br2-TIPS-Pn nanoparticles, exclusively the latter). Scans were typically obtained with 1 nm steps, 0.1 s averaging time (or 0.2 s averaging for better signal-to-noise), and with the slits set for 2 nm bandpass.

Scanning Electron Microscopy. Scanning electron microscope (SEM) images were measured on a Quanta 250 FEG environmental SEM using an accelerating voltage of 30.00 kV. Nanoparticles were deposited on a 300 mesh copper grid coated on one side with a carbon film (CF300-Cu, Electron Microscopy Sciences).

Pump–Probe Spectroscopy. Femtosecond pump–probe measurements were performed with a 5 kHz regeneratively amplified Ti:sapphire laser system (Spectra-Physics, Santa Clara, CA) driving a custom-built[71] noncollinear optical parametric amplifier (NOPA).[72] The laser system consists of a Ti:sapphire oscillator that seeds a Nd:YLF-pumped Ti:sapphire-based regenerative amplifier delivering ~150 fs pulses at ~800 nm with an average power of ~3 W. About 1.5 W is used to drive the NOPA. The NOPA was tuned to amplify regions of the seed continuum such that the output beam peaked at either ~530 or ~590 nm (Figure S1, Supporting Information). The NOPA pulses were compressed with a combination[73] of a folded 4-*f* grating compressor and single-prism pulse compressor.[74] A beamsplitter in the NOPA beam path served to generate separate pump and probe beams; the pump and probe pulse energies were controlled with a combination of a $\lambda/2$ waveplate and cube polarizer of similar composition and thickness such that the amount of material in pump and probe beam paths was approximately the same. Pulse compression was guided by optimizing either the nonresonant response of methanol or the polarization-gated frequency-resolved optical gating[75] signal obtained from water contained in a cuvette located at the sample position. Typical pulse durations were ~21 fs or less as assayed via the full width at half-maximum assuming a Gaussian pulse envelope (see Figure S1). Measurements of singlet fission time constants were performed with pump and probe polarizations oriented at the magic angle. Anisotropy data were obtained by performing successive measurements with the probe polarization set parallel and perpendicular relative to the pump polarization. More specific details on the optical configuration of the pump–probe spectrometer and associated electronics can be found in a recent report by McClure et al.[76] The solutions were contained in a 1 mm path length glass spectrophotometer cell (Starna Cells, Inc., Atascadero, CA); the optical density of the samples was kept at or below ~0.1 and 0.3 in the vicinity of the green and orange NOPA spectra, respectively. The pump beam spot size was estimated by measuring the power of the pump beam both in full and when passing through a 50 μm diameter pinhole (Newport, Irvine, CA). Pump fluences were determined with the estimated pump beam spot size and the pump power measured immediately prior the sample. Pump fluences are reported where appropriate. The total fraction of light absorbed by the sample, used to determine the absorbed pump fluence, was obtained by summing over the product of the sample spectrum in units of absorptance (i.e., 1 − T), which represents the fraction of light absorbed by the sample,[77] and the NOPA spectrum in units of intensity (i.e., counts per second), the latter scaled such that the integrated area was unity.

Single-Crystal X-ray Diffraction. The crystal structures of TIPS- and Br2-TIPS-Pn have been reported previously.[78,79] Structures of TSBS-, TIBS-, and F8-NODIPS-Pn were determined using Cu Kα radiation on a Bruker-Nonius X8 Proteum CCD diffractometer. The structures were solved and refined using SHELX programs.[80] Crystal handling followed procedures developed for manipulating fragile, sensitive samples.[81] Non-hydrogen atoms were refined with anisotropic displacement parameters, and hydrogens were included using riding models. The relatively high R-values for TSBS- and TIBS-Pn are a consequence of extensive disorder and twinning, respectively. In such cases, the spatial quality of the fit can help distinguish between problems caused by poor counting statistics and those caused by inadequate models.[82]

■ RESULTS AND DISCUSSION

Nanoparticle Preparation and Characterization. The core structures and side chains of TIPS-, TSBS-, TIBS-, F8-NODIPS-, and Br2-TIPS-Pn are shown in Figure 1a. Nanoparticles of the Pn derivatives were prepared by flash repreciptation.[48,49,64] Briefly, a solution of the compound
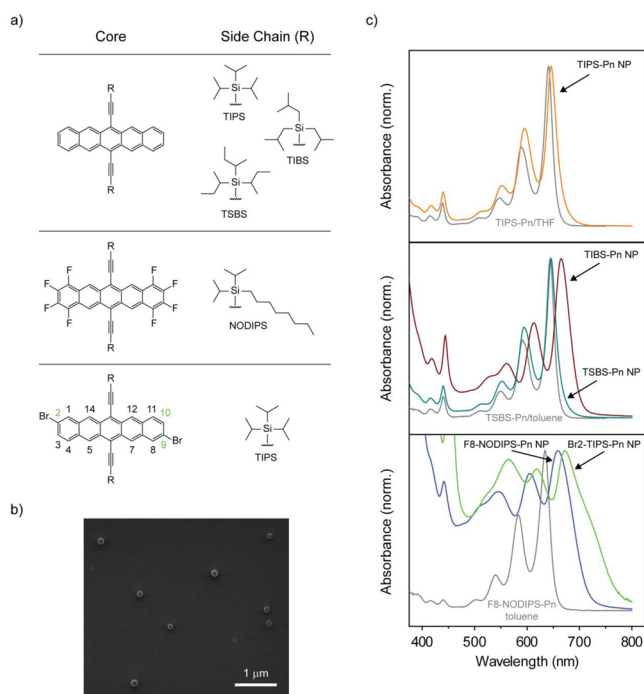

Figure 1. Pentacene derivatives and their nanoparticles. (a) Core structure and side chains (including acronyms) of the pentacene derivatives. (b) SEM image of ~100 nm diameter TIBS-pentacene nanoparticles. (c) Steady-state absorption spectra of TIPS-pentacene in THF and aqueous colloidal TIPS-pentacene nanoparticles (top panel), TSBS-pentacene in toluene and aqueous colloidal TSBS- and TIBS-pentacene nanoparticles (middle), and F8-NODIPS-pentacene in toluene and aqueous colloidal F8-NODIPS- and Br2-TIPS-pentacene nanoparticles (bottom panel). The absorption spectra of TIBS- and Br2-TIPS-pentacene in toluene have been omitted for clarity. The TIPS- and TSBS-pentacene nanoparticle absorption spectra exhibit a slight redshift relative to the absorption spectrum of the corresponding pentacene derivative dissolved in either THF or toluene. The TIBS-, F8-NODIPS-, and Br2-TIPS-pentacene nanoparticle absorption spectra are more substantially red-shifted and exhibit broader spectral features. Splitting of the 0−0 band in the Br2-TIPS-pentacene nanoparticle absorption spectrum is apparent.

dissolved in a "good" solvent (THF) was rapidly injected into a larger volume of a "bad" solvent (water). Taking TIBS-Pn as a representative example, we found this method produced approximately spherical nanoparticles with an average diameter of ~100 nm (Figure 1b). We determined an intensity-weighted mean (Z-average) diameter of ~69, ~76, ~94, ~98, and ~81 nm for the TIPS-, TSBS-, TIBS-, F8-NODIPS-, and Br2-TIPS-Pn nanoparticles, respectively, via dynamic light scattering measurements (Figures S2 and S3). The aqueous colloidal Pn derivative nanoparticles were stable over the course of at least one month when stored in the dark, i.e., no significant chemical decomposition was apparent (Figure S4). The only changes observed during this period of time were a wavelength-independent decrease in optical density that coincided with sample precipitation.

As a means of characterizing interactions between chromophores in the nanoparticles, we measured their steady-state electronic absorption spectra. We found that the absorption spectrum of an aqueous colloidal suspension of TIPS-Pn nanoparticles exhibits very little change relative to a dilute solution of the compound in THF (Figure 1c). The transition at 641 nm (1.93 eV) is assigned, in Platt's notation,

to the short-axis polarized ^1L_a transition.[83−87] The spectra exhibit vibronic structure; the 0−0, 0−1, and 0−2 bands of the ^1L_a transition of TIPS-Pn in THF exhibit a peak spacing of ~1350 cm^{-1} (~0.17 eV). The progressional intensities of the ^1L_a and ^1L_b bands in polyacenes are associated with two types of vibrational modes, namely, CCC bending and Kekulé-type CC stretching modes, grouped at ~250−500 and ~1400 cm^{-1}, respectively.[88−90] We observe only a slight redshift and broadening of the lowest-energy singlet transition in the TIPS-Pn nanoparticles relative to the chromophore dissolved in THF. The lack of significant change to the absorption spectrum indicates that the TIPS-Pn nanoparticles comprise primarily weakly interacting chromophores. In order to clarify the origin of the redshift of the lowest-energy singlet transition in the TIPS-Pn nanoparticles, we performed a solvatochromism study of the ^1L_a transition of TIPS-Pn (more details in the Supporting Information). Briefly, we find that the solvent environment representative of the bulk of the nanoparticle is most similar to toluene, as might be anticipated by the similarity of toluene and the Pn core. Similar to the TIPS-Pn nanoparticles, TSBS-Pn nanoparticles have an absorption spectrum that closely resembles that of a dilute solution of the chromophore dissolved in toluene (Figure 1c).

In contrast to the absorption spectra of the TIPS- and TSBS-Pn nanoparticles, the absorption spectrum of TIBS-Pn nanoparticles exhibited a comparatively larger redshift in the lowest-energy singlet transition. To determine the origin of the large redshift of the lowest-energy singlet transition in the TIBS-Pn nanoparticles, we monitored their absorption spectra as a function of time following injection of the TIBS-Pn/THF solution (Figure 2). The absorption spectrum measured
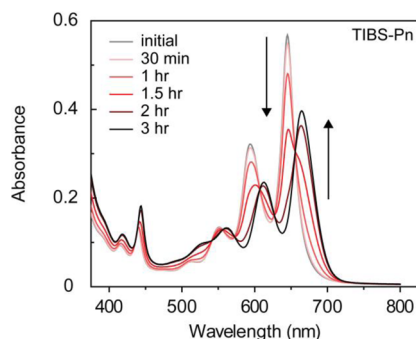

Figure 2. Electronic absorption spectra of aqueous colloidal TIBS-pentacene nanoparticles as a function of time following injection of the TIBS-pentacene/THF solution. There are a number of isosbestic points in the 0−0, 0−1, and 0−2 bands of the lowest-energy singlet transition that highlight the interconversion of two distinct populations: a population of weakly coupled chromophores and a population of more strongly coupled chromophores.

immediately following injection more closely resembles that of the dissolved chromophore, indicating a lack of electronic coupling between chromophores. Thereafter, the spectrum begins to change as residual good solvent (THF) evaporates from the water-based suspension. This interpretation is supported by experiments indicating that the final nanoparticle absorption spectrum is the same irrespective of the means of driving off the residual THF (Figure S6).[91] A number of isosbestic points appear in the TIBS-Pn nanoparticle absorption spectra that are most apparent in the vicinity of the 0−0, 0−1, and 0−2 bands of the lowest-energy singlet transition,

indicating interconversion between two distinct populations. To determine the identity of these two populations, we fit the intermediate time spectra of the TIBS-Pn nanoparticles with a linear combination of the initial (weakly coupled chromophore) and final (more strongly coupled chromophore) spectra (Figure S7). The fidelity of this analysis demonstrates that the spectral changes we observe clearly come from the interconversion of an initial population consisting of primarily weakly interacting chromophores to a final population consisting primarily of more strongly interacting chromophores.

Nanoparticles of the halogenated Pn derivatives, F8-NODIPS- and Br2-TIPS-Pn, also exhibited distinctively different absorption spectra compared with the corresponding derivatives dissolved in toluene (Figure 1c). Similar to TIBS-Pn, a comparatively large redshift of the lowest-energy singlet transition is observed (with respect to that observed for the TIPS- and TSBS-Pn nanoparticles). The F8-NODIPS- and Br2-TIPS-Pn nanoparticles also undergo a population interconversion as residual THF evaporates from the solution (Figure 3). The kinetics of interconversion are slightly faster and slower for the fluorinated and brominated derivative, respectively. Nanoparticles of the brominated derivative exhibit a second, slower period of change particularly noticeable in the 0−0 band where splitting is clearly evident. These observations indicate that,
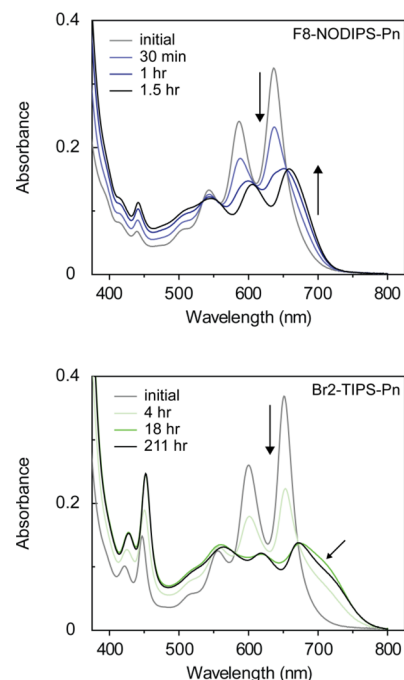

Figure 3. Electronic absorption spectra of aqueous colloidal F8-NODIPS- and Br2-TIPS-pentacene nanoparticles as a function of time following injection of the pentacene derivative/THF solution. Similar to the TIBS-pentacene nanoparticles, nanoparticles composed of these pentacene derivatives undergo an interconversion of a population of weakly coupled chromophores and a population of more strongly coupled chromophores. The kinetics of the interconversion are slightly faster in the case of F8-NODIPS-pentacene nanoparticles and slower in the case of Br2-TIPS-pentacene nanoparticles. We note that the "initial" spectrum reported for the F8-NODIPS-pentacene nanoparticles might include a nonzero contribution from the population of more strongly coupled chromophores as a result of the faster population interconversion kinetics.

similar to the TIBS-Pn nanoparticles, nanoparticles of the halogenated Pn derivatives evolve into nanoparticles that comprise primarily more strongly coupled chromophores.

We can use the extent of the redshift of the lowest-energy singlet transition of the nanoparticles relative to the dilute solution of the corresponding Pn derivative in toluene as an estimate of the strength of interaction between constituent chromophores in the nanoparticles. In the case of the TIPS- and TSBS-Pn nanoparticles, we observe a small redshift of ~80 and ~50 cm^{-1}, respectively. We ascribe the apparent redshift observed in these nanoparticles as largely a result of overlapping bands due to inhomogeneous broadening. As such, the magnitude of the redshift may not accurately reflect the strength of coupling between chromophores in the TIPS- and TSBS-Pn nanoparticles. In the case of the TIBS- and F8-NODIPS-Pn nanoparticles, we observe a redshift of ~490 and ~590 cm^{-1}, respectively. Davydov splitting[92–94] in the absorption spectrum of Br2-TIPS-Pn nanoparticles complicates the calculation of the redshift for nanoparticles of this compound, but fitting the two peaks comprising the 0–0 band with Gaussian functions results in a peak shift and splitting of ~1080 and ~1020 cm^{-1}, respectively (Figure S8).[95] Here, we ascribe the comparatively larger redshift observed in the TIBS-, NODIPS-, and Br2-TIPS-Pn nanoparticles as excitonic in nature and assert that the extent of the redshift more accurately reflects the strength of interaction between chromophores. The redshift of the lowest-energy singlet transition in the Pn derivative nanoparticles is accompanied by broadening in all cases, especially in the nanoparticles that comprise a large population of more strongly coupled chromophores. The line widths of the lowest-energy singlet transition are ~570, ~510, ~740, and ~1360 cm^{-1} for TIPS-, TSBS-, TIBS-, and F8-NODIPS-Pn nanoparticles, respectively. The line widths of the Gaussian functions used to model the Br2-TIPS-Pn data are ~1200 cm^{-1}.

To gain further insight into the solid-state order within the nanoparticles, we compared the absorption spectra of the nanoparticles with the absorption spectra of drop-cast films (Figure S9). Drop casting is the most common way to prepare crystalline films of the pentacene derivatives,[96] enabling us to compare the absorption spectra of the nanoparticles to that of crystalline material. While the TIPS- and TSBS-Pn nanoparticle absorption spectra resemble the chromophore dissolved in toluene, the TIBS-, F8-NODIPS-, and Br2-TIPS-Pn nanoparticle absorption spectra more closely resemble that of the drop-cast films. This indicates that nanoparticles of TIBS-, F8-NODIPS-, and Br2-TIPS-Pn comprise chromophores that exhibit relatively strong electronic interactions that likely adopt the same molecular packing configuration found in their respective drop-cast films. In the case of the TIPS- and TSBS-Pn nanoparticles, the lack of an excitonic redshift indicates that the majority of the chromophores within the nanoparticles do not exhibit significant electronic interactions, and thus the bulk of the nanoparticle cannot resemble the solid-state order in the crystals.[97]

To clarify following discussion, we categorize the nanoparticles prepared from the different Pn derivatives into two types: (i) those that comprise primarily weakly coupled chromophores that lack bulk structural order resembling the single-crystal arrangement, and (ii) those that comprise primarily more strongly coupled chromophores with a packing motif similar to that found in the single crystal. TIPS- and TSBS-Pn nanoparticles are classified as Type I, whereas TIBS-, F8-NODIPS-, and Br2-TIPS-Pn nanoparticles are classified as Type II.

Singlet Fission in Nanoparticles of Pentacene Derivatives. *Overview.* To investigate the fate of photo-excitations in these systems, we performed steady-state fluorescence measurements on aqueous suspensions of the nanoparticles. Nanoparticles of each Pn derivative exhibit very little fluorescence, which is in stark contrast to dilute solutions of the corresponding Pn derivatives. Using oxazine 1 in ethanol as a relative fluorescence quantum yield (FQY) standard,[98] we find that the FQY varies between 0.24 and 0.36 for TIPS-, TSBS-, TIBS-, F8-NODIPS-, and Br2-TIPS-Pn dissolved in THF (Table S2). In contrast, aqueous colloidal nanoparticles of the Pn derivatives are nearly nonemissive, exhibiting FQY values of ~1 × 10^{-4} or less (Table S2). These results indicate that a significant nonradiative decay pathway is present in the nanoparticles that is not present in a dilute solution of the respective Pn derivative.

To investigate the origin of this nonradiative decay pathway, we monitored the dynamics of both singlet and triplet populations with pump–probe spectroscopy. We first turn to the transient spectra of TIPS-Pn nanoparticles as this compound is known to undergo singlet fission.[30,99–103] The transient spectra of TIPS-Pn nanoparticles exhibit both positive- and negative-going spectral features (Figure 4a). The positive features at ca. 650 and 600 nm represent ground-state bleaching of the 0–0 and 0–1 vibronic bands, respectively; the transient feature associated with the 0–0 vibronic band has an additional contribution from stimulated emission. The negative features result from a photoinduced absorption (PIA) in either the singlet or triplet manifold. The modulation of the spectra at early pump–probe time delay arises from interference of the probe with scattered pump light. The transient spectra of dilute solutions of TIPS-Pn exhibit a broad PIA appearing below ca. 580 nm (Figure S10) that, on the basis of the relatively high FQY and previous assignments,[99,100] we assign to a singlet PIA. Because the transient spectra of the dilute solution of TIPS-Pn and nanoparticles of TIPS-Pn are similar on the earliest resolvable time scales, these results indicate a predominant population of singlet excitons in the TIPS-Pn nanoparticles immediately following photoexcitation. We find that the singlet PIA in the nanoparticles, however, subsequently decays quite rapidly.

The decay of the singlet PIA coincides with the growth of a spectral feature at ~508 nm. We assign this spectral feature to a triplet PIA of TIPS-Pn.[99,104] We note that the transient spectra of the TIPS-Pn nanoparticles at ~200 fs and ~10 ps very closely match those reported for the singlet and triplet transient species observed in dilute and concentrated solutions of TIPS-Pn in chloroform, respectively.[100] Biexponential fits to both the singlet PIA decay and the triplet PIA growth result in time constants on the order of a few hundred fs and a few ps, respectively (Figure 4b). Because the population of triplets through intersystem crossing is negligible in TIPS-Pn on these time scales,[100] singlet fission represents the most probable triplet formation pathway.

The transient spectra of nanoparticles of TIPS-, TSBS-, TIBS-, F8-NODIPS-, and Br2-TIPS-Pn derivatives all exhibit the same overall qualitative features and trends (Figure S11). Namely, we observe singlet-like transient spectra near the time origin of the experiment and subsequently resolve the concomitant loss and growth of singlet and triplet features, respectively. These observations indicate that singlet fission
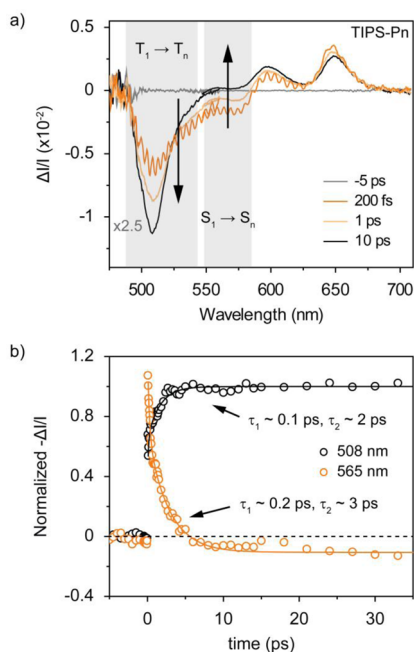
Figure 4. Pump−probe measurements on aqueous colloidal suspensions of TIPS-pentacene nanoparticles. (a) Transient absorption spectra of TIPS-pentacene nanoparticles dispersed in water as a colloidal suspension. The distinct transient spectral features associated with singlet and triplet states are highlighted in gray. The singlet photoinduced absorption is broad and extends from ca. 500 to 580 nm, while the triplet photoinduced absorption exhibits a relatively more intense and narrow line shape peaking at ca. 508 nm in TIPS-pentacene nanoparticles. These data were acquired from independent experiments with two different NOPA spectra; the data below 560 nm were scaled to match the data above ca. 540 nm by matching the signal intensity in the region of 540 to 560 nm. Pump−probe time delays are indicated in the legend. (b) Temporal evolution of singlet and triplet photoinduced absorption features for TIPS-pentacene nanoparticles that exhibit a rapid, concomitant loss and growth, respectively. These data were taken as the mean over the wavelengths 495 to 520 nm and 550 to 580 nm for the triplet and singlet photoinduced absorption, respectively. The kinetics traces were fit with biexponential functions with associated time constants indicated. The fits begin at a pump−probe time delay of ~100 fs to avoid overlap near the time origin of the experiment where the coherent spike, unaccounted for in these measurements, could potentially introduce artifacts into the data. The absorbed (incident) fluence was ≤12 (100) $\mu J/cm^2$.

occurs in nanoparticles of each Pn derivative. We highlight that the excitation conditions for these experiments resulted in several hundred singlet excitons per nanoparticle (the interested reader is referred to the Supporting Information for more details on this estimation). Because of the large nanoparticle volume, this corresponds to a mean distance of no less than approximately eight nanometers between the photogenerated singlet excitons (Table S3). We also note that the peak of the triplet PIA transition shifts in the nanoparticles from ~508 nm for TIPS- and TSBS-Pn to ~516 nm for TIBS- and F8-NODIPS-Pn to ~536 nm for Br2-TIPS-Pn. These shifts of the PIA are consistent with more extensive orbital overlap between molecules in the nanoparticles in the series of TIPS-Pn ≈ TSBS-Pn < TIBS-Pn ≤ F8-NODIPS-Pn < Br2-TIPS-Pn.

Intriguingly, we find the time necessary for the transient triplet spectral feature to form depends on the structure of the Pn derivative (Figure 5 and Table 1). We attempted to model
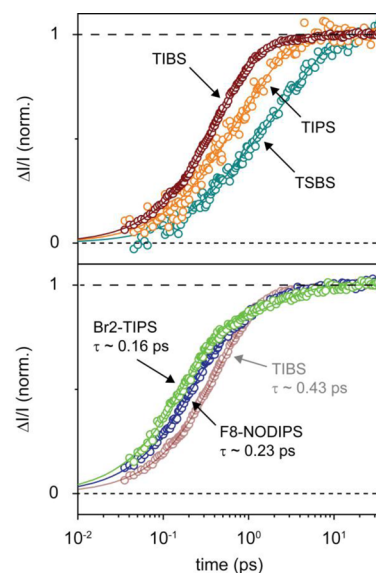

Figure 5. Temporal evolution of the triplet photoinduced absorption appearing in TIPS-, TSBS-, TIBS-, F8-NODIPS-, and Br2-TIPS-pentacene nanoparticle transient spectra. Temporal evolution of the triplet PIA appearing in the transient spectra of the TIPS-, TSBS-, and TIBS-pentacene nanoparticles (upper panel). The overall rate of triplet formation, as determined by the time scale of the triplet PIA growth, depends on the side chain of the pentacene derivative. Temporal evolution of the triplet PIA appearing in the transient spectra of the F8-NODIPS- and Br2-TIPS-pentacene nanoparticles (lower panel). The TIBS-pentacene data from the upper panel have been reproduced and overlaid for comparison. The time constant associated with triplet pair formation, as determined by the first component of the triplet PIA growth, is indicated. The data and associated fits have been offset and normalized to facilitate comparison. The data and associated fits were offset by the signal amplitude at the time origin, as estimated by extrapolating the fit to the time origin, and were subsequently normalized to the signal amplitude between 20 and 40 ps. The data in the region of pump−probe pulse overlap have been omitted for clarity. The absorbed (incident) pump fluences in these measurements was maintained ≤3 (30) $\mu J/cm^2$.

Table 1. Coefficients and Time Constants of a Biexponential Fit to the Growth of the Triplet Photoinduced Absorption Signal Amplitude[a]

	T PIA, $1 - e^{-1}$ buildup time			
Pn derivative	A_1 (%)	τ_1, (ps)	A_2 (%)	τ_2, (ps)
TIPS	0.34 ± 0.07	0.22 ± 0.05	0.66 ± 0.07	1.37 ± 0.03
TSBS	0.37 ± 0.09	0.7 ± 0.4	0.63 ± 0.09	3.6 ± 0.9
TIBS	0.91 ± 0.02	0.43 ± 0.01	0.09 ± 0.02	3 ± 1
F8-NODIPS	0.77 ± 0.05	0.23 ± 0.03	0.23 ± 0.05	1.7 ± 0.3
Br2-TIPS	0.78 ± 0.04	0.16 ± 0.03	0.22 ± 0.04	2.0 ± 0.6

[a]The amplitude of the triplet photoinduced absorption was taken as the mean over the spectral range 500−520, 495−520, 505−525, 505−525, and 520−550 nm for the TIPS-, TSBS-, TIBS-, F8-NODIPS-, and Br2-TIPS-pentacene nanoparticles, respectively. These data were obtained by averaging over at least four measurements obtained from two separate sample preparations. The limits represent an analysis of a single standard deviation of the time constants obtained from these fits. The absorbed (incident) pump fluences in the measurements included in this analysis were maintained ≤2 (30) $\mu J/cm^2$ for the TIPS- and TSBS-pentacene nanoparticles and ≤6 (50) $\mu J/cm^2$ for the TIBS-, F8-NODIPS-, Br2-TIPS-pentacene nanoparticles.

these data with a single exponential, but found that a biexponential function provides a better representation (Figure S12). There are several possible physical origins of non-exponential triplet formation kinetics, including singlet fission through high-lying excited states, singlet fission through molecular packing arrangements with varying degrees of electronic coupling, and multiple phases of triplet formation including energy-migration limited singlet fission.[36] These various physical processes that could contribute to triplet formation will now be discussed for the Type I and II nanoparticles; the interested reader is referred to the Supporting Information for a more detailed discussion of nonexponential singlet fission kinetics.

Type I Nanoparticles. As a first step toward differentiating between various means of generating triplets through singlet fission, we measured the sensitivity of the nanoparticle triplet formation kinetics to pump fluence. Triplet formation kinetics in nanoparticles of TIPS-Pn are relatively insensitive to absorbed pump fluence (Figure 6) indicating that singlet fission through high-lying excited singlet states is not responsible for the observed nonexponential kinetics. Although we did not explicitly measure the fluence dependence of the triplet formation kinetics in the case of the TSBS-Pn nanoparticles, we consider the relative insensitivity of the triplet formation kinetics to pump fluence in nanoparticles of TIPS-Pn to be sufficient to rule out singlet fission through high-lying excited states in nanoparticles composed of either compound.

To begin to understand the relevance of various molecular packing arrangements on singlet fission in Type I nanoparticles, we recall and highlight the ~508 nm peak position of the triplet PIA appearing in the TIPS- and TSBS-Pn nanoparticle transient spectra (see Figure S11). Previous reports on a highly concentrated solution of TIPS-Pn[100] and polycrystalline films of TIPS-Pn[30,101,102] indicate that the triplet PIA peak appears at ~508 and ~525−530 nm, respectively. The triplet transient spectra of nanoparticles composed of TIPS- and TSBS-Pn are most similar to those reported for highly concentrated solutions of TIPS-Pn. This comparison suggests that singlet fission in nanoparticles composed of TIPS- and TSBS-Pn occurs largely at sites best represented by pairs of molecules rather than crystalline domains. The opposite conclusion can be drawn in the case of TIBS-, F8-NODIPS-, and Br2-TIPS-Pn nanoparticles that exhibit substantially red-shifted triplet transient spectra more similar in character to those reported for crystalline films of TIPS-Pn. A large body of reports indicate that Pn and its derivatives are capable of undergoing rapid singlet fission in a variety of molecular packing arrangements.[30,33,101,102] The complete quenching of singlet photoexcitations through singlet fission in highly concentrated solutions of TIPS-Pn[100] suggests that rapid and efficient singlet fission through pairs of molecules exhibiting a distribution of packing arrangements might be possible. This is because the diffusive encounter of two molecules in an isotropic solution is expected to give rise to a distribution of encounter geometries. Taken together, it would not be surprising if a convolution of the time constants associated with singlet fission through pairs of Pn derivatives exhibiting a distribution of packing arrangements was on the order of a picosecond or less. We therefore cannot rule out singlet fission through various (including a distribution of) molecular packing arrangements in nanoparticles of TIPS- and TSBS-Pn and conclude that the
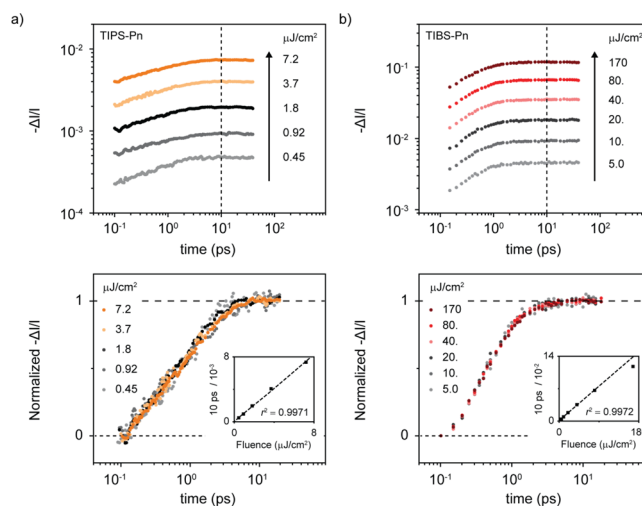

Figure 6. Fluence dependence of triplet photoinduced absorption appearing in TIPS- and TIBS-pentacene nanoparticle transient spectra. (a) Log−log plot of the signal amplitude of the triplet PIA appearing in TIPS-pentacene nanoparticle transient spectra for several absorbed fluences ranging from 0.45 to 7.2 $\mu J/cm^2$ (upper panel). The dashed line demarcates the pump−probe time delay at which the linearity of the triplet PIA signal amplitude is assessed in the inset of the bottom panel. Semilog plot of triplet PIA signal amplitude for several incident fluences offset such that the signal amplitude at 100 fs is equivalent and normalized to the mean over the time range of 5 to 20 ps (bottom panel). Absorbed pump fluences ($\mu J/cm^2$) are indicated in the legend. Triplet PIA signal amplitude measured at a pump−probe time delay of 10 ps plotted against incident pump fluence (bottom panel, inset). Overlaying the data is a linear fit with $r^2 = 0.9971$. (b) Log−log plot of the signal amplitude of the triplet PIA appearing in TIBS-pentacene nanoparticle transient spectra for several absorbed fluences ranging from 5.0 to 170 $\mu J/cm^2$ (upper panel). The dashed line demarcates the pump−probe time delay at which the linearity of the triplet PIA signal amplitude is assessed in the inset of the bottom panel. Semilog plot of triplet PIA signal amplitude for several incident fluences offset such that the signal amplitude at 100 fs is equivalent and normalized to the mean over the time range of 5 to 20 ps (bottom panel). Absorbed pump fluences ($\mu J/cm^2$) are indicated in the legend. Triplet PIA signal amplitude measured at a pump−probe time delay of 10 ps plotted against incident pump fluence (bottom panel, inset). Overlaying the data is a linear fit to the first five data points, with $r^2 = 0.9972$. A linear fit including all six data points gave $r^2 = 0.9860$. An r^2 value deviating from unity by more than 1% was taken as an indicator of nonlinearity.

majority of singlet fission takes place at sites consisting of pairs of molecules in nanoparticles composed of these compounds.

Another possible contributor to the observed nonexponential triplet formation kinetics is a component associated with energy-migration limited singlet fission,[25] where we make the distinction here between energy transfer, an elementary step, and energy migration, a series of energy transfers.[105] To test the role of energy migration in these systems, we monitored the depolarization of the 0−0 ground-state bleach feature appearing in the pump−probe spectrum (Figure S14). Depolarization of photoexcited chromophores has been shown to be a sensitive probe of energy migration in the solid state.[106] In the case of TIPS- and TSBS-Pn nanoparticles, we find that the initial anisotropy value of ~0.4 decays rapidly to a nonzero offset with a time constant of ~1 ps. The observation of a rapid decay of the anisotropy on a picosecond time scale is consistent with energy migration in a disordered, condensed phase medium.[106]

The pump−probe anisotropy measurements enable further clarification of the extent of solid-state order in the nano-

particles. In brief, the data indicate that the TIPS- and TSBS-Pn nanoparticles (Type I) have little long-range order whereas the TIBS-Pn nanoparticles (Type II) exhibit extensive long-range solid-state order. The interested reader is referred to the Supporting Information for additional details.

We now discuss the overall time scale of triplet formation to facilitate determination of the relative significance of the two physical processes described above that could contribute to triplet formation in the TIPS- and TSBS-Pn nanoparticles. For comparison, we calculate an amplitude average time constant[107] of 1.0 ± 0.1 and 2.5 ± 0.6 ps for the TIPS- and TSBS-Pn nanoparticle triplet formation kinetics, respectively (Table 1). The overall slower triplet formation kinetics observed in the case of TSBS-Pn nanoparticles likely result from a lower concentration of singlet fission sites. This can be inferred from a slightly smaller net absorbance appearing to the red of the 0−0 band of the lowest-energy singlet transition in TSBS- relative to the TIPS-Pn nanoparticles (Figure S15). The lower concentration of singlet fission sites observed in nanoparticles of TSBS-Pn might arise from the variability in packing motifs adopted by this mixture of diastereomers coupled with the larger, denser solubilizing groups held closer to the chromophore that inhibit close intermolecular contacts (Figure S16). In this context, the lower concentration of singlet fission sites would not be expected to alter the *intrinsic* rate of singlet fission; however, it does support the interpretation of inhibited π-stacking of this compound in the solid state. Variability in the distribution of molecular packing motifs will, however, influence triplet formation kinetics. Alternatively, a lower initial exponential burst along with an increased triplet formation time constant associated with energy-migration limited singlet fission[25] could also explain the slower triplet formation kinetics observed in nanoparticles of TSBS-Pn. A lower concentration of singlet fission sites would result in a smaller initial component of triplet formation as well as require a longer period of time for energy to migrate to fission sites, the latter supposition being supported by energy migration studies on various concentrations of perylene diimide derivatives embedded in polymer host matrices.[108] Because the time scale of triplet formation is nearly equivalent to the time scale of the anisotropy depolarization in the TIPS-Pn nanoparticles (see Figure S14), energy migration might be the rate-determining step in these nanoparticles. On the basis of this observation, we suggest that triplet formation in both TIPS- and TSBS-Pn nanoparticles exhibits a non-negligible contribution from the migration of energy to a subset of sites where singlet fission occurs.

In sum, while it is difficult to ascribe triplet formation in nanoparticles of TIPS- and TSBS-Pn to a particular physical process, we can exclude singlet fission through high-lying singlet states as a contributor to triplet formation. Triplet formation in these systems is attributed to singlet fission through pairs of molecules exhibiting a distribution of packing arrangements, multiple phases of triplet formation including energy-migration limited singlet fission, or a combination of these two processes. The observation of singlet fission in nanoparticles that lack long-range solid-state order, including those composed of a Pn derivative exhibiting inhibited π-stacking in the solid state, highlights the remarkable versatility of Pn derivatives as singlet fission chromophores.

Type II Nanoparticles. Similar to the Type I nanoparticles, we find that the triplet formation kinetics in the TIBS-Pn nanoparticles are remarkably insensitive to pump fluence

(Figure 6), allowing us once again to exclude singlet fission through high-lying excited states. The linearity of the signal to absorbed fluences as high as ~100 μJ/cm^2 is particularly striking. Singlet−singlet annihilation and other high-order annihilation processes are well-known excitation deactivation pathways in molecular media.[19,109−119] The linearity of the triplet PIA signal at absorbed pump fluences as high as ~100 μJ/cm^2 in the TIBS-Pn nanoparticles suggests that singlet fission is much faster than high-order annihilation processes such as singlet−singlet annihilation.

In contrast to TIPS- and TSBS-Pn nanoparticles, nanoparticles of TIBS-, F8-NODIPS-, and Br2-TIPS-Pn all exhibit rapid, predominantly subpicosecond kinetics associated with the triplet transient feature (Table 1). The vast majority of the biexponential fit is associated with the first, faster time constant, for example, with corresponding amplitudes of 0.91 ± 0.02, 0.77 ± 0.05, and 0.78 ± 0.04 for TIBS-, NODIPS-F8-, and Br2-TIPS-Pn nanoparticles, respectively. We rule out singlet fission through multiple molecular packing arrangements as a contributor to the triplet formation kinetics in TIBS-, F8-NODIPS-, and Br2-TIPS-Pn nanoparticles on the basis of the large population of more strongly coupled chromophores (see Figures 2, S9, and 3) and apparently less nonexponential triplet formation kinetics. For example, while the triplet formation kinetics of the Type I nanoparticles are not clearly biexponential (i.e., several other functions could conceivably describe these data), the triplet formation kinetics of the Type II nanoparticles are fit very well with the sum of two exponentials, one of which is associated the majority of the amplitude of the growth. We rule out multiple phases of triplet formation including energy-migration limited singlet fission on the basis of these observations, as well.

We attribute the first, faster time constant to triplet pair formation in the TIBS-, F8-NODIPS-, and Br2-TIPS-Pn nanoparticles. For TIBS-, F8-NODIPS-, and Br2-TIPS-Pn nanoparticles we measure values of 0.43 ± 0.01, 0.23 ± 0.03, and 0.16 ± 0.03 ps, respectively, indicating that triplet pair formation is most rapid in nanoparticles of Br2-TIPS-Pn (Table 1). The latter, slower time constant likely represents a residual energy migration component, vibrational cooling (with associated changes to the transient spectra), or changes in the transient signal resulting from the separation of the triplet pair into isolated, localized triplets. The values we measure for this latter, slower time constant are 3 ± 1, 1.7 ± 0.3, and 2.0 ± 0.6 ps for TIBS-, F8-NODIPS-, and Br2-TIPS-Pn nanoparticles, respectively (Table 1). Although we are unable to definitively distinguish between vibrational cooling and triplet pair separation with conventional transient absorption techniques, the slower time constant might indicate subtle changes to the transient spectra associated with the separation of the triplet pair into isolated, localized triplets. These changes are most notable in the Br2-TIPS-Pn nanoparticles. An isosbestic point is present in the transient spectra acquired at pump−probe time delays of 1 and 10 ps, for example, along with a slight redshift of the triplet PIA peak maximum (see Figure S11). Recent electric field assisted pump−probe measurements by Kandada et al. on polycrystalline films of Pn support this interpretation.[120]

Effect of Molecular Packing on Singlet Fission Dynamics. In order to more clearly understand the effect of molecular arrangement on singlet fission, we use the molecular packing arrangement derived from the crystal structures of TIBS-, F8-NODIPS-, and Br2-TIPS-Pn as an approximation of the molecular packing arrangement adopted in nanoparticles of

these compounds. This assumption was tested by (i) comparing the absorption spectra of the nanoparticles with the absorption spectra of drop-cast films (see Figure S9), and (ii) comparing the X-ray diffractogram of a pentacene derivative nanoparticle powder with that of the corresponding crystalline powder along with the diffractogram predicted from the single crystal structure (see Supporting Information for a more detailed discussion).

In the single crystal, TIBS-Pn crystallizes with the space group $P\bar{1}$ ($a = 5.898$, $b = 14.187$, $c = 26.421$; $\alpha = 78.673$, $\beta = 84.728$, $\gamma = 84.507°$). The molecular packing arrangement adopted in the single crystal indicates that adjacent TIBS-Pn molecules are displaced by 5.0 and 0.2 Å along their short and long axes, respectively (Figure 7, Table S4). The observation of
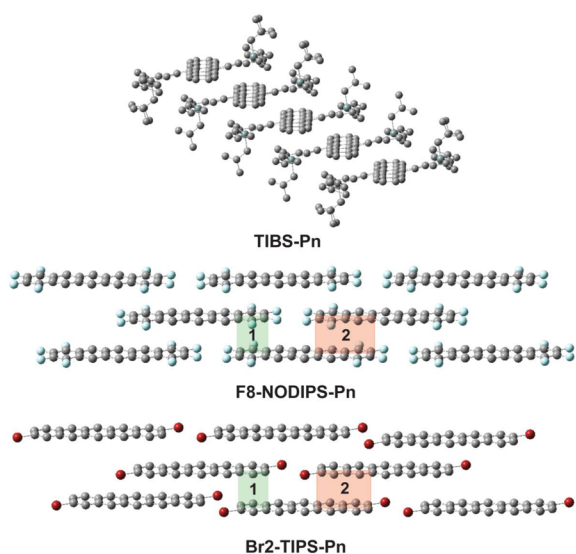

Figure 7. Proposed solid-state order in TIBS-, F8-NODIPS, and Br2-TIPS-pentacene nanoparticles. The solid-state order derived from the single crystal data is displayed. Each unique pair of molecules present in the F8-NODIPS- and Br2-TIPS-pentacene crystal structure that could potentially facilitate singlet fission is highlighted. The solid-state order for the 2,9- and 2,10-dibromo pentacene derivatives are overall very similar and therefore only that of the 2,9-dibromo pentacene derivative is shown for clarity. Hydrogen atoms as well as side chains of the halogenated pentacene derivatives have been omitted for clarity.

subpicosecond triplet pair formation in nanoparticles of this derivative is thus quite remarkable given the extent of displacement along the molecular short axis (Figure S19). We note that the short-axis displacement appears to place the peripheral triple bond of one functionalized pentacene directly on top of the pentacene core of an adjacent molecule. Our preliminary theoretical calculations indicate that the triple bond helps to mediate orbital overlap between adjacent molecules (Figure S20), suggesting that direct spatial overlap of neighboring pentacene cores is not a requirement for singlet fission in TIBS-Pn, a result that is likely applicable to alkyne-substituted acene derivatives in general.

Both halogenated derivatives crystallize with the same triclinic $P\bar{1}$ space group as TIPS-Pn, with nonzero short-axis slip and significant long-axis displacement between pairs of molecules.[78] From the crystal structures of F8-NODIPS- and Br2-TIPS-Pn, it is apparent that there are two unique pairs of molecules possessing different long- and short-axis displacement distances (Figure 7, Table S4). Such molecular pairs are

also found within the same "bricklayer" packing motif in TIPS-Pn single crystals (ref 78). In order to assess the molecular pair most favorable for singlet fission, we turn to a recent report by Wang et al. for guidance on comparing the feasibility of various molecular short- and long-axis displacements on singlet fission dynamics.[33] Guided by these data, we anticipate that molecular pair 2 with less displacement along the long axis should exhibit more favorable triplet pair formation kinetics (see Table S4 for specific molecular packing distances).

Reports in the literature indicate that triplet pair formation occurs in polycrystalline films of TIPS-Pn with a time constant varying somewhere between ∼100 and 400 fs,[30,101−103] although we note that Ramanan et al. originally reported a value of ∼1 ps.[99] The precise value depends upon the details of the associated sample preparation, transient absorption measurements, and data analysis. Taking the time constant measured in the majority of cases (i.e., 100 to 400 fs) as that representative of the time constant associated with triplet pair formation in crystalline TIPS-Pn, we compare this with the ∼230 fs triplet pair formation time constant measured in the nanoparticles of F8-NODIPS-Pn. According to the calculations of Wang et al. on model Pn pairs,[33] we anticipate that, for a fixed short-axis displacement of 0.9 Å, increased displacement along the molecular long axis of 6.7 to 7.5 Å should lead to a significantly *decreased* rate of triplet pair formation (or increased time constant). We find, however, that while the time constant we measure is within the range of values measured for TIPS-Pn, the time constant is not significantly *increased* as predicted by the calculations.[33]

We now turn to a comparison of the effect of differences in displacement along the molecular short and long axes on the time scale of triplet pair formation in nanoparticles of F8-NODIPS- and Br2-TIPS-Pn. According to calculations based on the model Pn pair,[33] we expect that increased long- and short-axis displacement (i.e., for a pair of molecules exhibiting a short-axis displacement of ∼0.9 relative to 1.0 Å and long-axis displacement of ∼7.5 relative to ∼7.7 Å) would lead to a *decreased* rate of triplet pair formation. Intriguingly, we find that the rate of triplet pair formation in nanoparticles of Br2-TIPS-Pn is *increased* (i.e., the triplet pair formation time constant decreases from ∼230 fs for F8-NODIPS-Pn nanoparticles to ∼160 fs for Br2-TIPS-Pn nanoparticles), which is again contrary to what is predicted.[33]

Thus, we have utilized a series of Pn derivatives to facilitate a direct comparison of the effect of different molecular packing arrangements on singlet fission rates. This is particularly notable for the halogenated Pn derivatives[70] as they possess *different* side-chain substituents, yet adopt an overall similar molecular packing arrangement. Significantly, we find that our results are in qualitative disagreement with those predicted for a model Pn pair.[33] While representing a suitable first-order estimate of singlet fission rates, we suggest that the discrepancy observed here between experiment and theory is a result of long-range effects, including exciton delocalization and the associated relative admixture of charge-transfer configurations in the description of the exciton wave function,[43] that are not incorporated into theoretical models based on molecular pairs. Bardeen and co-workers, for example, recently noted that exciton delocalization may cause the electronic interaction terms that govern singlet fission rates to become less sensitive to individual molecular positions.[45]

Excitonic Effects and Singlet Fission Dynamics. We end with a brief discussion of excitonic effects on singlet fission

dynamics. We find that the extent of the redshift of the lowest-energy singlet transition in the TIBS-, F8-NODIPS-, and Br2-TIPS-Pn nanoparticles, in addition to other associated changes to their absorption spectra, correlates with an increasing rate of singlet fission. Van Voorhis, Friend, and co-workers have suggested that a large, red-shifted transition indicates increased charge-transfer mixing into the bright lowest-energy exciton state of polyacenes.[30] This is asserted, in part, on the basis of theoretical work on a series of polyacenes,[121] including Pn,[121−123] that predicts a substantial admixture of charge-transfer excitations into the lowest singlet exciton states in crystals of these compounds. These reports suggest that exciton delocalization, coincident with a large relative admixture of charge-transfer configurations into the exciton wave function,[43] plays a role in facilitating rapid singlet fission.[124] Indeed, the role of orbital overlap, introduced into models via charge-transfer configurations, in mediating single-step singlet fission is generally recognized.[2,16]

In order to gauge the extent to which charge-transfer configurations contribute to the lowest-energy singlet exciton wave function, we assess the degree to which the absorption strength of the more strongly coupled chromophores is attenuated relative to the weakly coupled chromophores in nanoparticles of TIBS-, F8-NODIPS-, and Br2-TIPS-Pn (Figure 8). As the extent to which charge-transfer configurations contribute to the overall description of the exciton wave function increases, the oscillator strength of the transition is expected to decrease,[43,125] and this should result in a lower extinction coefficient. Assuming that the extinction coefficient of the weakly coupled chromophores is similar for the different Pn derivatives (and given that the experiments were performed on samples of unaltered concentration contained in a spectrophotometer cell with an equivalent path length), we can utilize the magnitude of their absorbance as a relative internal standard to facilitate comparison between samples. We find that the nanoparticles that comprise primarily more strongly coupled chromophores absorb less strongly (i.e., their extinction coefficient has decreased) relative to the nanoparticles that comprise largely weakly coupled chromophores at the peak of the 0−0 band of the lowest-energy singlet transition and that the scaled absorbance magnitude of the TIBS-Pn aggregate (∼70%) is less than that of the F8-NODIPS-Pn aggregate (∼50%) which is less than that of the Br2-TIPS-Pn aggregate (∼40%). These results suggest that charge-transfer configurations contribute more to the lowest-energy singlet exciton wave function when the exciton is more delocalized. Thus, we have provided experimental evidence that exciton delocalization is coincident with an increased relative admixture of charge-transfer configurations in the exciton wave function and that this correlates with rapid singlet fission.

To test the generality of our observations, we investigated singlet fission dynamics in nanoparticles composed of two halogenated Hn derivatives (Figure S21). The lowest-energy singlet transition in each case is red-shifted by ∼1000−1100 cm^{-1} with respect to a dilute solution of the corresponding chromophore in THF, indicating a large population of more strongly coupled chromophores, similar to the Type II nanoparticles of the Pn derivatives. Using pump−probe spectroscopy, we measure a time constant of roughly 400 fs for singlet fission in each of the halogenated Hn derivative nanoparticles (Figure S22). Interestingly, films of polycrystal-line Hn studied by Busby et al. possess a significant redshift of the lowest-energy singlet transition (∼2500 cm^{-1}) and a similar
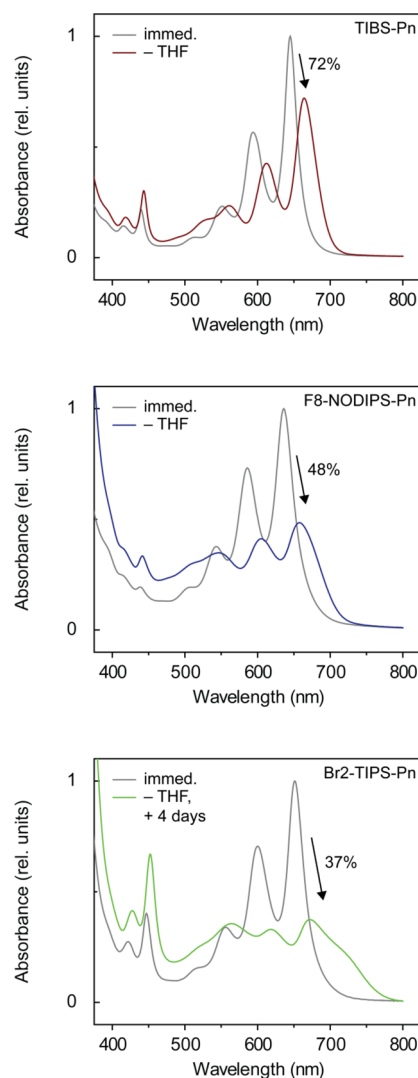

Figure 8. Electronic absorption spectra of TIBS-, F8-NODIPS-, and Br2-TIPS-pentacene nanoparticles immediately after injection of the pentacene derivative/THF solution and following the complete interconversion of weak and more strongly coupled chromophore populations. Each data set was scaled relative to the maximum of the 0−0 band of the lowest-energy singlet transition of the "immed." spectrum. Compared with the respective nanoparticles that comprise primarily weakly coupled chromophores (i.e., the "immed." spectrum), the magnitude of the absorbance at the peak of the 0−0 band of the lowest-energy singlet transition decreases in the series of the TIBS-, F8-NODIPS-, and Br2-TIPS-pentacene aggregates decreases to ∼72, 48, and 37%, respectively. Assuming that the extinction coefficient of the weakly coupled chromophores is similar for the different pentacene derivatives (and given that the experiments were performed on samples of unaltered concentration contained in a spectrophotometer cell with an equivalent path length), these data indicate that the extinction coefficient at the peak of the 0−0 band of the lowest-energy singlet transition of the Br2-TIPS-pentacene aggregate is attenuated to the greatest degree.

singlet fission time constant (530 fs).[24] In contrast, Lee et al. reported a time constant of ∼5.1 ps for singlet fission in thin films of a tricyclohexylsilylethynyl-substituted Hn derivative.[126] Significantly, these films exhibited at least an order-of-magnitude smaller redshift of the lowest-energy singlet transition, suggesting that they comprise primarily weakly coupled chromophores. Thus, it is apparent that weak excitonic

interactions correlate with significantly slower rates of singlet fission whereas strong excitonic interactions correlate with rapid singlet fission. The fact that similar structure–function relationships are obtained in solids of the Pn and Hn derivatives studied here further suggest that strong excitonic interactions generally promote rapid singlet fission in these systems.

As chromophore coupling and exciton energy are inextricably linked,[42,127] another critical factor to consider that affects the singlet fission rate is energy level matching, i.e., $2E(T_1) - E(S_1)$.[2] An example can found in tetracene and its derivatives.[19,25,30,64] Coupling between chromophores in crystalline tetracene is quite strong and, as a consequence, singlet fission is endoergic and quite slow (ca. 100 ps).[19,30] In contrast, solids of 5,12-diphenyltetracene comprise a large population of weakly coupled chromophores where singlet fission is exoergic and the process can be quite fast (ca. 1 ps).[25,64]

The Pn and Hn derivatives studied in this work all exhibit exoergic singlet fission; in the Hn derivatives, the exoergicity is anticipated to be quite significant. The comparatively "fast" and "slow" singlet fission rates observed in the Type II nanoparticles composed of Pn and Hn derivatives are consistent with the microscopic theory of singlet fission developed by Berkelbach, Reichman, and co-workers that predicts a turnover of the rate with increasing exoergicity on account of the excess electronic energy that must be dissipated through the strongly coupled vibrational degrees of freedom.[24] The successively larger singlet fission rates observed in nanoparticles of the Pn derivatives could also be interpreted within a similar framework whereby decreasing exoergicity leads to successively larger singlet fission rates. We note, however, that the energy of the lowest singlet exciton of TIBS- and F8-NODIPS-Pn nanoparticles is quite similar, suggesting that (with the assumption that the triplet exciton energies do not change considerably) differences in energy level alignment alone might not suffice to describe the different observed singlet fission rates. Indeed, recently reported work on covalently tethered Pn dimers with similar exciton energies, yet different coupling exhibit widely varying singlet fission rates (varying over two orders-of-magnitude).[41]

■ CONCLUSIONS

We reported a study of the singlet fission dynamics in nanoparticles of five Pn derivatives. Nanoparticles of TIPS- and TSBS-Pn comprise primarily weakly coupled chromophores that are capable of undergoing singlet fission in the absence of bulk structural order. This is particularly notable for TSBS-Pn that, from an analysis of the single crystal, does not exhibit a strong propensity to π-stack. Nanoparticles of TIBS-, F8-NODIPS-, and Br2-TIPS-Pn, on the other hand, comprise primarily chromophores exhibiting stronger electronic coupling as evidenced by their excitonically red-shifted absorption spectra. Nanoparticles of these Pn derivatives exhibit order approaching that of the bulk crystal and rapid, subpicosecond triplet pair formation. This is the case even for TIBS-Pn, a Pn derivative exhibiting displacement extensive enough along the molecular short axis that adjacent pentacene cores do not overlap; orbital overlap, in this case, appears to be mediated by the triplet bond introduced through alkyne-substitution. We utilize the molecular packing arrangement derived from the single crystal to compare the observed rates of triplet pair formation to those predicted by current theoretical models based on individual Pn pairs. We find notable discrepancies

between experiment and theory and suggest that the origin of the discrepancies arise from long-range effects, including exciton delocalization and the associated relative admixture of charge-transfer configurations in the description of the exciton wave function, not incorporated into models based on molecular pairs. For example, we measure the fastest triplet pair formation in nanoparticles of Br2-TIPS-Pn that also exhibit the largest excitonic redshift and most drastic reduction of the extinction coefficient associated with the 0–0 band of the lowest-energy singlet transition. Additionally, we observe rapid singlet fission in nanoparticles of two halogenated hexacene derivatives. This can similarly be attributed to strong excitonic interactions.

Several general conclusions emerge from this work:

(i) Pn derivatives are versatile singlet fission chromophores capable of undergoing singlet fission in the absence of bulk structural order where singlet fission most likely occurs through pairs of molecules exhibiting various packing arrangements (e.g., nanoparticles of TIPS- and TSBS-Pn). Nanoparticles of Pn derivatives exhibit singlet fission even in the case where the molecules exhibit inhibited π-stacking in the solid state (e.g., TSBS-Pn). Our observations further underscore the remarkable versatility of Pn derivatives as singlet fission chromophores.[30,33,41,99–103] Roberts, Bradforth and co-workers previously reported efficient singlet fission in largely amorphous solids of 5,12-diphenyltetracene;[25,64] a comparison with the results of that work, specifically the kinetics of triplet formation and magnitude of the triplet yield, would suggest an appreciable triplet yield in nanoparticles of the acene derivatives investigated here.

(ii) Halogenation of organic semiconductors has recently been demonstrated to be an effective tool to enhance intermolecular electronic coupling as well as both electron and hole transport in organic thin films.[70,128–133] Our discovery of rapid, subpicosecond triplet pair formation in nanoparticles of halogenated Pn and Hn derivatives, likely as a result of their propensity to assemble in the solid state with strongly π-stacked packing arrangements, suggests that halogenation of singlet fission chromophores may also represent a promising new design strategy to promote solid-state order appropriate for rapid singlet exciton fission. We highlight that incorporation of halogen atoms into prototypical singlet fission chromophores,[66,67,134] such as tetracene,[128–130] pentacene,[70] hexacene,[131] and perylene diimide derivatives,[132,133] for example, has been shown to promote solid-state order while retaining the slip-stacked packing arrangement between individual pairs of molecules that is generally anticipated to facilitate rapid and efficient singlet fission.[2,16]

(iii) Exciton delocalization, coincident with an increased admixture of charge-transfer configurations in the description of the exciton wave function, may facilitate more rapid singlet fission. We have reported and correlated several experimental observables in the present work supporting this interpretation, which is consistent with the general consensus emerging from contemporary theoretical models of singlet fission.[24,30,135] We suggest that incorporating aspects of exciton delocalization[43,45] into theoretical models investigating the effect of various molecular packing arrangements on singlet fission dynamics[32,33] represents a necessary challenge.[33]

ASSOCIATED CONTENT

Ⓢ Supporting Information

Additional synthetic, experimental, and theoretical details as well as data, including laser pulse characterization, dynamic light scattering measurements, steady-state absorption and fluorescence measurements, fluorescence quantum yield measurements, transient absorption and anisotropy measurements, analysis of crystallographic data, X-ray diffractograms, and molecular orbitals for a pair of functionalized pentacenes. Crystallographic data have been deposited with the Cambridge Crystallographic Data Centre (TSBS-Pn, CCDC 1038341; TIBS-Pn, CCDC 1038342; F8-NODIPS-Pn, CCDC 1038343). The Supporting Information is available free of charge on the ACS Publications website at DOI: 10.1021/ja512668r.

AUTHOR INFORMATION

Corresponding Authors
*anthony@uky.edu
*dseferos@chem.utoronto.ca
*gscholes@princeton.edu

Present Address
#Department of Chemistry, Texas A&M University, College Station, Texas 77842, United States.

Author Contributions
‖R.D.P. and A.J.T. contributed equally to this work.

Notes
The authors declare no competing financial interest.

ACKNOWLEDGMENTS

REFERENCES

(1) Swenberg, C. E.; Geacintov, N. E. In *Organic Molecular Photophysics*; Birks, J. B., Ed.; Wiley-Interscience: Hoboken, NJ, 1973; Vol. *1*, pp 489−564.

(2) Smith, M. B.; Michl, J. *Chem. Rev.* **2010**, *110*, 6891−6936.

(3) Piland, G. B.; Burdett, J. J.; Dillon, R. J.; Bardeen, C. J. *J. Phys. Chem. Lett.* **2014**, *5*, 2312−2319.

(4) Shockley, W.; Queisser, H. J. *J. Appl. Phys.* **1961**, *32*, 510−519.

(5) Dexter, D. L. *J. Lumin.* **1979**, *18−19*, 779−784.

(6) Hanna, M. C.; Nozik, A. J. *J. Appl. Phys.* **2006**, *100*, 074510.

(7) Nozik, A. J. In *Photoelectrochemical Water Splitting: Materials, Processes and Architectures*; Lewerenz, H.-J., Peter, L., Eds.; RSC Publishing: Cambridge, U.K., 2013; pp 359−388.

(8) Rao, A.; Wilson, M. W. B.; Hodgkiss, J. M.; Albert-Seifried, S.; Bässler, H.; Friend, R. H. *J. Am. Chem. Soc.* **2010**, *132*, 12698−12703.

(9) Chan, W.-L.; Ligges, M.; Jailaubekov, A.; Kaake, L.; Miaja-Avila, L.; Zhu, X.-Y. *Science* **2011**, *334*, 1541−1545.

(10) Ehrler, B.; Wilson, M. W. B.; Rao, A.; Friend, R. H.; Greenham, N. C. *Nano Lett.* **2012**, *12*, 1053−1057.

(11) Ehrler, B.; Walker, B. J.; Böhm, M. L.; Wilson, M. W. B.; Vaynzof, Y.; Friend, R. H.; Greenham, N. C. *Nat. Commun.* **2012**, *3*, 1019.

(12) Chan, W.-L.; Tritsch, J. R.; Zhu, X.-Y. *J. Am. Chem. Soc.* **2012**, *134*, 18295−18302.

(13) Tritsch, J. R.; Chan, W.-L.; Wu, X.; Monahan, N. R.; Zhu, X.-Y. *Nat. Commun.* **2013**, *4*, 2679.

(14) Jadhav, P. J.; Brown, P. R.; Thompson, N.; Wunsch, B.; Mohanty, A.; Yost, S. R.; Hontz, E.; Van Voorhis, T.; Bawendi, M. G.; Bulović, V.; et al. *Adv. Mater.* **2012**, *24*, 6169−6174.

(15) Congreve, D. N.; Lee, J.; Thompson, N. J.; Hontz, E.; Yost, S. R.; Reusswig, P. D.; Bahlke, M. E.; Reineke, S.; Voorhis, T. V.; Baldo, M. A. *Science* **2013**, *340*, 334−337.

(16) Smith, M. B.; Michl, J. *Annu. Rev. Phys. Chem.* **2013**, *64*, 361−386.

(17) Paci, I.; Johnson, J. C.; Chen, X.; Rana, G.; Popović, D.; David, D. E.; Nozik, A. J.; Ratner, M. A.; Michl, J. *J. Am. Chem. Soc.* **2006**, *128*, 16546−16553.

(18) Burdett, J. J.; Müller, A. M.; Gosztola, D.; Bardeen, C. J. *J. Chem. Phys.* **2010**, *133*, 144506.

(19) Burdett, J. J.; Gosztola, D.; Bardeen, C. J. *J. Chem. Phys.* **2011**, *135*, 214508.

(20) Thompson, N. J.; Wilson, M. W. B.; Congreve, D. N.; Brown, P. R.; Scherer, J. M.; Bischof, T. S.; Wu, M.; Geva, N.; Welborn, M.; Voorhis, T. V.; et al. *Nat. Mater.* **2014**, *13*, 1039−1043.

(21) Lee, J.; Jadhav, P.; Baldo, M. A. *Appl. Phys. Lett.* **2009**, *95*, 033301.

(22) Wilson, M. W. B.; Rao, A.; Clark, J.; Kumar, R. S. S.; Brida, D.; Cerullo, G.; Friend, R. H. *J. Am. Chem. Soc.* **2011**, *133*, 11830−11833.

(23) Tabachnyk, M.; Ehrler, B.; Gélinas, S.; Böhm, M. L.; Walker, B. J.; Musselman, K. P.; Greenham, N. C.; Friend, R. H.; Rao, A. *Nat. Mater.* **2014**, *13*, 1033−1038.

(24) Busby, E.; Berkelbach, T. C.; Kumar, B.; Chernikov, A.; Zhong, Y.; Hlaing, H.; Zhu, X.-Y.; Heinz, T. F.; Hybertsen, M. S.; Sfeir, M. Y.; et al. *J. Am. Chem. Soc.* **2014**, *136*, 10654−10660.

(25) Roberts, S. T.; McAnally, R. E.; Mastron, J. N.; Webber, D. H.; Whited, M. T.; Brutchey, R. L.; Thompson, M. E.; Bradforth, S. E. *J. Am. Chem. Soc.* **2012**, *134*, 6388−6400.

(26) Wang, C.; Tauber, M. J. *J. Am. Chem. Soc.* **2010**, *132*, 13988−13991.

(27) Johnson, J. C.; Nozik, A. J.; Michl, J. *J. Am. Chem. Soc.* **2010**, *132*, 16302−16303.

(28) Schrauben, J. N.; Ryerson, J. L.; Michl, J.; Johnson, J. C. *J. Am. Chem. Soc.* **2014**, *136*, 7363−7373.

(29) Eaton, S. W.; Shoer, L. E.; Karlen, S. D.; Dyar, S. M.; Margulies, E. A.; Veldkamp, B. S.; Ramanan, C.; Hartzler, D. A.; Savikhin, S.; Marks, T. J.; et al. *J. Am. Chem. Soc.* **2013**, *135*, 14701−14712.

(30) Yost, S. R.; Lee, J.; Wilson, M. W. B.; Wu, T.; McMahon, D. P.; Parkhurst, R. R.; Thompson, N. J.; Congreve, D. N.; Rao, A.; Johnson, K.; et al. *Nat. Chem.* **2014**, *6*, 492−497.

(31) Turro, N. J.; Scaiano, J. C.; Ramamurthy, V. *Modern Molecular Photochemistry of Organic Molecules*; University Science Books: Sausalito, CA, 2010.

(32) Renaud, N.; Sherratt, P. A.; Ratner, M. A. *J. Phys. Chem. Lett.* **2013**, *4*, 1065−1069.

(33) Wang, L.; Olivier, Y.; Prezhdo, O. V.; Beljonne, D. *J. Phys. Chem. Lett.* **2014**, *5*, 3345−3353.

(34) Müller, A. M.; Avlasevich, Y. S.; Müllen, K.; Bardeen, C. J. *Chem. Phys. Lett.* **2006**, *421*, 518−522.

(35) Müller, A. M.; Avlasevich, Y. S.; Schoeller, W. W.; Müllen, K.; Bardeen, C. J. *J. Am. Chem. Soc.* **2007**, *129*, 14240−14250.

(36) Johnson, J. C.; Nozik, A. J.; Michl, J. *Acc. Chem. Res.* **2013**, *46*, 1290−1299.

(37) Burdett, J. J.; Bardeen, C. J. Acc. Chem. Res. **2013**, 46, 1312–1320.

(38) Johnson, J. C.; Akdag, A.; Zamadar, M.; Chen, X.; Schwerin, A. F.; Paci, I.; Smith, M. B.; Havlas, Z.; Miller, J. R.; Ratner, M. A.; et al. J. Phys. Chem. B **2013**, 117, 4680–4695.

(39) Lefler, K. M.; Brown, K. E.; Salamant, W. A.; Dyar, S. M.; Knowles, K. E.; Wasielewski, M. R. J. Phys. Chem. A **2013**, 117, 10333–10345.

(40) Margulies, E. A.; Shoer, L. E.; Eaton, S. W.; Wasielewski, M. R. Phys. Chem. Chem. Phys. **2014**, 16, 23735–23742.

(41) Zirzlmeier, J.; Lehnherr, D.; Coto, P. B.; Chernick, E. T.; Casillas, R.; Basel, B. S.; Thoss, M.; Tykwinski, R. R.; Guldi, D. M. Proc. Natl. Acad. Sci. U. S. A. **2015**, 112, 5325–5330.

(42) Scholes, G. D.; Rumbles, G. Nat. Mater. **2006**, 5, 683–696.

(43) Scholes, G. D. ACS Nano **2008**, 2, 523–537.

(44) Harcourt, R. D.; Scholes, G. D.; Ghiggino, K. P. J. Chem. Phys. **1994**, 101, 10521–10525.

(45) Dillon, R. J.; Piland, G. B.; Bardeen, C. J. J. Am. Chem. Soc. **2013**, 135, 17278–17281.

(46) Ryerson, J. L.; Schrauben, J. N.; Ferguson, A. J.; Sahoo, S. C.; Naumov, P.; Havlas, Z.; Michl, J.; Nozik, A. J.; Johnson, J. C. J. Phys. Chem. C **2014**, 118, 12121–12132.

(47) Monahan, N.; Zhu, X.-Y. Annu. Rev. Phys. Chem. **2015**, 66, 601–618.

(48) Kasai, H.; Nalwa, H. S.; Oikawa, H.; Okada, S.; Matsuda, H.; Minami, N.; Kakuta, A.; Ono, K.; Mukoh, A.; Nakanishi, H. Jpn. J. Appl. Phys. **1992**, 31, L1132–L1134.

(49) Kim, H. Y.; Bjorklund, T. G.; Lim, S.-H.; Bardeen, C. J. Langmuir **2003**, 19, 3941–3946.

(50) Veerman, M.; Resendiz, M. J. E.; Garcia-Garibay, M. A. Org. Lett. **2006**, 8, 2615–2617.

(51) Kuzmanich, G.; Natarajan, A.; Chin, K. K.; Veerman, M.; Mortko, C. J.; Garcia-Garibay, M. A. J. Am. Chem. Soc. **2008**, 130, 1140–1141.

(52) Kuzmanich, G.; Gard, M. N.; Garcia-Garibay, M. A. J. Am. Chem. Soc. **2009**, 131, 11606–11614.

(53) Simoncelli, S.; Kuzmanich, G.; Gard, M. N.; Garcia-Garibay, M. A. J. Phys. Org. Chem. **2010**, 23, 376–381.

(54) Kuzmanich, G.; Xue, J.; Netto-Ferreira, J.-C.; Scaiano, J. C.; Platz, M.; Garcia-Garibay, M. A. Chem. Sci. **2011**, 2, 1497–1501.

(55) Kuzmanich, G.; Garcia-Garibay, M. A. J. Phys. Org. Chem. **2011**, 24, 883–888.

(56) Kuzmanich, G.; Vogelsberg, C. S.; Maverick, E. F.; Netto-Ferreira, J. C.; Scaiano, J. C.; Garcia-Garibay, M. A. J. Am. Chem. Soc. **2012**, 134, 1115–1123.

(57) Doan, S. C.; Kuzmanich, G.; Gard, M. N.; Garcia-Garibay, M. A.; Schwartz, B. J. J. Phys. Chem. Lett. **2012**, 3, 81–86.

(58) Nielsen, A.; Kuzmanich, G.; Garcia-Garibay, M. A. J. Phys. Chem. A **2014**, 118, 1858–1863.

(59) Lim, S.-H.; Bjorklund, T. G.; Spano, F. C.; Bardeen, C. J. Phys. Rev. Lett. **2004**, 92, 107402.

(60) Chin, K. K.; Natarajan, A.; Gard, M. N.; Campos, L. M.; Shepherd, H.; Johansson, E.; Garcia-Garibay, M. A. Chem. Commun. **2007**, 41, 4266–4268.

(61) Lebedeva, N. V.; Tarasov, V. F.; Resendiz, M. J. E.; Garcia-Garibay, M. A.; White, R. C.; Forbes, M. D. E. J. Am. Chem. Soc. **2010**, 132, 82–84.

(62) Kuzmanich, G.; Simoncelli, S.; Gard, M. N.; Spänig, F.; Henderson, B. L.; Guldi, D. M.; Garcia-Garibay, M. A. J. Am. Chem. Soc. **2011**, 133, 17296–17306.

(63) Wang, C.; Berg, C. J.; Hsu, C.-C.; Merrill, B. A.; Tauber, M. J. J. Phys. Chem. B **2012**, 116, 10617–10630.

(64) Mastron, J. N.; Roberts, S. T.; McAnally, R. E.; Thompson, M. E.; Bradforth, S. E. J. Phys. Chem. B **2013**, 117, 15519–15526.

(65) Musser, A. J.; Maiuri, M.; Brida, D.; Cerullo, G.; Friend, R. H.; Clark, J. J. Am. Chem. Soc. **2015**, 137, 5130–5139.

(66) Anthony, J. E. Chem. Rev. **2006**, 106, 5028–5048.

(67) Anthony, J. E. Angew. Chem., Int. Ed. **2008**, 47, 452–483.

(68) Anthony, J. E. In Organic Electronics; Klauk, H., Ed.; Wiley-VCH: Weinheim, 2006; pp 58–74.

(69) Anthony, J. E.; Eaton, D. L.; Parkin, S. R. Org. Lett. **2002**, 4, 15–18.

(70) Swartz, C. R.; Parkin, S. R.; Bullock, J. E.; Anthony, J. E.; Mayer, A. C.; Malliaras, G. G. Org. Lett. **2005**, 7, 3163–3166.

(71) Turner, D. B.; Wilk, K. E.; Curmi, P. M. G.; Scholes, G. D. J. Phys. Chem. Lett. **2011**, 2, 1904–1911.

(72) Wilhelm, T.; Piel, J.; Riedle, E. Opt. Lett. **1997**, 22, 1494–1496.

(73) Fork, R. L.; Brito Cruz, C. H.; Becker, P. C.; Shank, C. V. Opt. Lett. **1987**, 12, 483–485.

(74) Akturk, S.; Gu, X.; Kimmel, M.; Trebino, R. Opt. Express **2006**, 14, 10101–10108.

(75) Trebino, R.; DeLong, K. W.; Fittinghoff, D. N.; Sweetser, J. N.; Krumbügel, M. A.; Richman, B. A.; Kane, D. J. Rev. Sci. Instrum. **1997**, 68, 3277–3295.

(76) McClure, S. D.; Turner, D. B.; Arpin, P. C.; Mirkovic, T.; Scholes, G. D. J. Phys. Chem. B **2014**, 118, 1296–1308.

(77) Tkachenko, N. V. Optical Spectroscopy: Methods and Instrumentations; Elsevier: Amsterdam, 2006.

(78) Anthony, J. E.; Brooks, J. S.; Eaton, D. L.; Parkin, S. R. J. Am. Chem. Soc. **2001**, 123, 9482–9483.

(79) Okamoto, T.; Jiang, Y.; Becerril, H. A.; Hong, S.; Senatore, M. L.; Tang, M. L.; Toney, M. F.; Siegrist, T.; Bao, Z. J. Mater. Chem. **2011**, 21, 7078–7081.

(80) Sheldrick, G. M. Acta Crystallogr., Sect. A: Found. Crystallogr. **2008**, 64, 112–122.

(81) Parkin, S.; Hope, H. J. Appl. Crystallogr. **1998**, 31, 945–953.

(82) Parkin, S. Acta Crystallogr., Sect. A: Found. Crystallogr. **2000**, 56, 157–162.

(83) Platt, J. R. J. Chem. Phys. **1949**, 17, 484–495.

(84) Birks, J. B. Photophysics of Aromatic Molecules; Wiley-Interscience: Hoboken, NJ, 1970.

(85) Birks, J. B. In Organic Molecular Photophysics; Birks, J. B., Ed.; Wiley-Interscience: Hoboken, NJ, 1973; Vol. 1, pp 1–55.

(86) Pope, M.; Swenberg, C. E. Electronic Processes in Organic Crystals and Polymers, 2nd ed.; Oxford University Press: Cambridge, U.K., 1999.

(87) The ^1L_a transition is assigned in accord with the energies and relative intensities expected for the different electronic bands for pentacene and its derivatives as outlined in ref 85.

(88) Ohno, K. Chem. Phys. Lett. **1978**, 53, 571–577.

(89) Ohno, K. J. Mol. Spectrosc. **1979**, 77, 329–348.

(90) Pentacenes functionalized with a trialkylsilylethynyl moiety have an additional totally symmetric stretching mode associated with the ethynyl group. See for example: Aragó, J.; Viruela, P. M.; Ortí, E.; Osuna, R. M.; Hernández, V.; Navarrete, J. T. L.; Swartz, C. R.; Anthony, J. E. Theor. Chem. Acc. **2011**, 128, 521.

(91) We also monitored the mass of the solution before and after injection of the TIBS-Pn/THF solution and observed a reduction of solution mass (interpreted as the loss primarily of residual THF from the injected solution) coincident with the changes in the absorption spectra.

(92) McRae, E. G.; Kasha, M. J. Chem. Phys. **1958**, 28, 721–722.

(93) Kasha, M. Rev. Mod. Phys. **1959**, 31, 162–169.

(94) Hochstrasser, R. M.; Kasha, M. Photochem. Photobiol. **1964**, 3, 317–331.

(95) The magnitude of the peak splitting is comparable to the magnitude of the Davydov splitting reported for Pn that ranges between ~1030 and ~1100 cm^{-1}. See for example: Yamagata, H.; Norton, J.; Hontz, E.; Olivier, Y.; Beljonne, D.; Brédas, J. L.; Silbey, R. J.; Spano, F. C. J. Chem. Phys. **2011**, 134, 204703.

(96) Coppo, P.; Yeates, S. G. Adv. Mater. **2005**, 17, 3001–3005.

(97) Ostroverkhova, O.; Shcherbyna, S.; Cooke, D. G.; Egerton, R. F.; Hegmann, F. A.; Tykwinski, R. R.; Parkin, S. R.; Anthony, J. E. J. Appl. Phys. **2005**, 98, 033701.

(98) Rurack, K.; Spieles, M. Anal. Chem. **2011**, 83, 1232–1242.

(99) Ramanan, C.; Smeigh, A. L.; Anthony, J. E.; Marks, T. J.; Wasielewski, M. R. J. Am. Chem. Soc. **2012**, 134, 386–397.

(100) Walker, B. J.; Musser, A. J.; Beljonne, D.; Friend, R. H. *Nat. Chem.* **2013**, *5*, 1019−1024.

(101) Herz, J.; Buckup, T.; Paulus, F.; Engelhart, J.; Bunz, U. H. F.; Motzkus, M. *J. Phys. Chem. Lett.* **2014**, *5*, 2425−2430.

(102) Wu, Y.; Liu, K.; Liu, H.; Zhang, Y.; Zhang, H.; Yao, J.; Fu, H. *J. Phys. Chem. Lett.* **2014**, *5*, 3451−3455.

(103) Musser, A. J.; Liebel, M.; Schnedermann, C.; Wende, T.; Kehoe, T. B.; Rao, A.; Kukura, P. *Nat. Phys.* **2015**, *11*, 352−357.

(104) Smith and Michl (ref 16) and Van Voorhis, Friend, and co-workers (ref 30) have suggested this spectral feature may be attributable to a T_1-T_3 transition.

(105) Ghiggino, K. P.; Smith, T. A. *Prog. React. Kinet.* **1993**, *18*, 375−436.

(106) Gaab, K. M.; Bardeen, C. J. *J. Phys. Chem. B* **2004**, *108*, 4619−4626.

(107) Sillen, A.; Engelborghs, Y. *Photochem. Photobiol.* **1998**, *67*, 475−486.

(108) Schlosser, M.; Lochbrunner, S. *J. Phys. Chem. B* **2006**, *110*, 6001−6009.

(109) Tolstoi, N. A.; Abramov, A. P. *Sov. Phys. Solid State* **1967**, *9*, 255.

(110) Babenko, S. D.; Benderskii, V. A.; Goldanskii, V. I.; Lavrushko, A. G.; Tychinskii, V. P. *Phys. Status Solidi B* **1971**, *45*, 91−97.

(111) Swenberg, C. E.; Geacintov, N. E.; Pope, M. *Biophys. J.* **1976**, *16*, 1447−1452.

(112) López-Delgado, R.; Miehée, J. A.; Sipp, B. *Opt. Commun.* **1976**, *19*, 79−82.

(113) Fleming, G. R.; Millar, D. P.; Morris, G. C.; Morris, J. M.; Robinson, G. W. *Aust. J. Chem.* **1977**, *30*, 2353−2359.

(114) Greene, B. I.; Millard, R. R. *Phys. Rev. Lett.* **1985**, *55*, 1331−1334.

(115) Schatz, G. H.; Brock, H.; Holzwarth, A. R. *Proc. Natl. Acad. Sci. U. S. A.* **1987**, *84*, 8414−8418.

(116) Sundström, V.; Gillbro, T.; Gadonas, R. A.; Piskarskas, A. *J. Chem. Phys.* **1988**, *89*, 2754−2762.

(117) Stevens, M. A.; Silva, C.; Russell, D. M.; Friend, R. H. *Phys. Rev. B: Condens. Matter Mater. Phys.* **2001**, *63*, 165213.

(118) Gélinas, S.; Kirkpatrick, J.; Howard, I. A.; Johnson, K.; Wilson, M. W. B.; Pace, G.; Friend, R. H.; Silva, C. *J. Phys. Chem. B* **2013**, *117*, 4649−4653.

(119) It was recently reported, for example, that high-order annihilation processes become effective in films of poly(9,9′-dioctylfluorene-*co*-benzothiadiazole) (colloquially known as F8BT) at fluences as low as several μJ/cm^2. See specifically: ref 118.

(120) Kandada, A. R. S.; Petrozza, A.; Lanzani, G. *Phys. Rev. B: Condens. Matter Mater. Phys.* **2014**, *90*, 075310.

(121) Yamagata, H.; Norton, J.; Hontz, E.; Olivier, Y.; Beljonne, D.; Brédas, J. L.; Silbey, R. J.; Spano, F. C. *J. Chem. Phys.* **2011**, *134*, 204703.

(122) Beljonne, D.; Yamagata, H.; Brédas, J. L.; Spano, F. C.; Olivier, Y. *Phys. Rev. Lett.* **2013**, *110*, 226402.

(123) Sharifzadeh, S.; Darancet, P.; Kronik, L.; Neaton, J. B. *J. Phys. Chem. Lett.* **2013**, *4*, 2197−2201.

(124) Elegant work by Berkelbach, Reichman and co-workers (ref 135) and Van Voorhis, Friend and co-workers (ref 30) indicates that there is a fundamental limit to the time scale of triplet pair formation, and the extent that additional admixture of charge-transfer configurations into the exciton wave function can facilitate rapid single fission, and that this time scale is determined by nuclear motions that facilitate the photophysical transformation (i.e., the adiabatic limit).

(125) Berkelbach, T. C.; Hybertsen, M. S.; Reichman, D. R. *J. Chem. Phys.* **2014**, *141*, 074705.

(126) Lee, J.; Bruzek, M. J.; Thompson, N. J.; Sfeir, M. Y.; Anthony, J. E.; Baldo, M. A. *Adv. Mater.* **2013**, *25*, 1445−1448.

(127) Scholes, G. D.; Ghiggino, K. P.; Oliver, A. M.; Paddon-Row, M. N. *J. Am. Chem. Soc.* **1993**, *115*, 4345−4349.

(128) Moon, H.; Zeis, R.; Borkent, E.-J.; Besnard, C.; Lovinger, A. J.; Siegrist, T.; Kloc, C.; Bao, Z. *J. Am. Chem. Soc.* **2004**, *126*, 15322−15323.

(129) Chen, Z.; Müller, P.; Swager, T. M. *Org. Lett.* **2006**, *8*, 273−276.

(130) Okamoto, T.; Nakahara, K.; Saeki, A.; Seki, S.; Oh, J. H.; Akkerman, H. B.; Bao, Z.; Matsuo, Y. *Chem. Mater.* **2011**, *23*, 1646−1649.

(131) Purushothaman, B.; Parkin, S. R.; Kendrick, M. J.; David, D.; Ward, J. W.; Yu, L.; Stingelin, N.; Jurchescu, O. D.; Ostroverkhova, O.; Anthony, J. E. *Chem. Commun.* **2012**, *48*, 8261−8263.

(132) Zugenmaier, P.; Duff, J.; Bluhm, T. L. *Cryst. Res. Technol.* **2000**, *35*, 1095−1115.

(133) Delgado, M. C. R.; Kim, E.-G.; da Silva Filho, D. A.; Bredas, J.-L. *J. Am. Chem. Soc.* **2010**, *132*, 3375−3387.

(134) Tang, M. L.; Bao, Z. *Chem. Mater.* **2011**, *23*, 446−455.

(135) Berkelbach, T. C.; Hybertsen, M. S.; Reichman, D. R. *J. Chem. Phys.* **2013**, *138*, 114103.